Coexistence of spin-orbit torque and unidirectional magnetoresistance effect induced by spin polarization with spin rotation symmetry in Co/Cu/Co structures

Shuling Sun,[*] Bo Wang,[*] Wangda Li, Xiaoxue Zeng, Yonghai Guo, Bo Han, Tao Wang,
Dezheng Yang, Xiaolong Fan, and Jiangwei Cao [†]

*Key Laboratory for Magnetism and Magnetic Materials of the Ministry of Education,
Lanzhou University, Lanzhou 730000, People's Republic of China*

The conventional spin-orbit torque (SOT) and magnetoresistance effect observed in normal-metal (NM)/ferromagnet (FM) bilayers originate from the interaction between magnetic moments and spin with in-plane transverse polarization ($\hat{\sigma}_y$). In FM/NM/FM trilayer structures, the presence of an extra FM layer breaks the symmetry, resulting in spin polarization other than $\hat{\sigma}_y$ and the corresponding SOT. However, the study on the unidirectional magnetoresistance (UMR) effect induced by the spin polarization with spin rotation (SR) symmetry is still missing. In this work, we investigate the SOT and UMR effect in a Co/Cu/Co structure with crossed anisotropy by utilizing the harmonic longitudinal voltage measurement. We demonstrate that, in addition to the harmonic terms originating from the fieldlike SOT of the spin polarization with spin Hall and SR symmetry, two different unidirectional harmonic signals are observed in the angular and field scan measurements. Further, combining the SOT effective fields results from the harmonic Hall voltage measurement, we successfully separate the contributions of the observed unidirectional harmonic signals, which include the dampinglike SOT contribution through the giant magnetoresistance effect, and the UMR induced by the spin current with different polarization directions through spin-dependent scattering mechanism.

I. INTRODUCTION

The interaction between spin of itinerant electrons and magnetic moments leads to the well-known spin torque effects and magnetoresistance (MR) effects in magnetic heterostructures. In early spin-valve structures, the current polarized in one ferromagnet (FM) layer passes through the spacer layer and exerts torque on the other FM layer, named the spin transfer torque (STT) effect [1–3]. The STT effect enables current-induced magnetization switching, domain wall motion, or magnetization oscillation in FM layers, and therefore has potential applications in magnetic random-access memory (MRAM), racetrack memory, and spin torque oscillators. The spin-orbit torque (SOT) effect [4–8] provides another way to manipulate magnetization by current based on several different physical mechanisms, including the spin Hall effect (SHE) in heavy metal [8–12], the Rashba-Edelstein effect (REE) at normal-metal (NM)/FM interface [13–16], topological surface states in topological insulators [17–19], and the anomalous Hall effect in FM [20–22], etc. In comparison to the STT effect, SOT exhibits several advantages in memory and oscillator applications, and therefore has invoked another upsurge in the study of spintronics.

The MR effect is another reflection of the interaction between spin and magnetic moment. In addition to the early discovery of the giant MR (GMR) effect [23,24] in magnetic

multilayers and the tunneling MR (TMR) [25] effect in magnetic tunnel junctions, the spin-Hall MR (SMR) [26–28] and unidirectional MR (UMR) [29–31] have been discovered in NM/FM bilayers in recent years. In the SMR scenario, the spin current produced by the SHE in the NM layer can be partially absorbed by the FM layer via the STT effect at the NM/FM interface. The unabsorbed spin current is reflected at the NM/FM interface and back converted to a charge current via inverse SHE (ISHE), leading to a resistance discrepancy in NM/FM bilayers between the parallel and perpendicular states of spin polarization and magnetization, which is named SMR. In addition, UMR reflects the resistance difference between the parallel and antiparallel states of spin polarization and magnetization. According to its different physical mechanism, the UMR effect can be divided into bulk or interfacial spin-dependent UMR and spin-flip UMR [31]. Among them, the UMR caused by the spin current with spin Hall (SH) symmetry through the spin scattering mechanism was also named unidirectional spin Hall magnetoresistance (USMR) [29]. The UMR has a potential application in MRAM as a simple readout method because it permits detection of the magnetization direction of a single FM layer without any additional FM pinned layer.

Based on the symmetry consideration, as a charge current is applied along the x direction in NM/FM bilayers, the spin polarization in the out-of-plane spin current is limited to the y direction ($\hat{\sigma}_y$). However, in FM_1/NM/FM_2 trilayer structures, the presence of an extra ferromagnetic layer breaks the symmetry as compared with the NM/FM bilayers, which enables spin currents with polarization other than $\hat{\sigma}_y$ and the

---

[*]These authors contributed equally to this work.
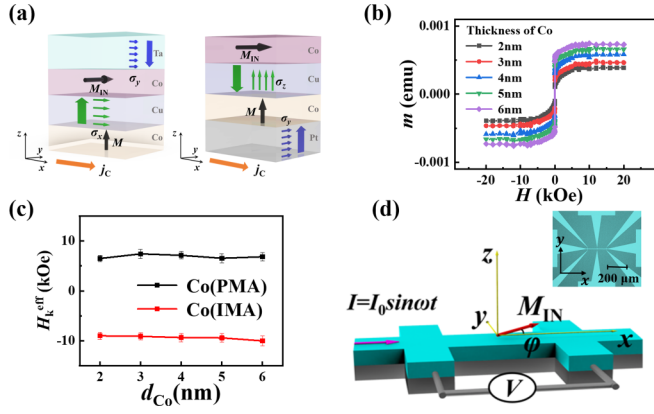[†]Corresponding author: caojw@lzu.edu.cn

FIG. 1. (a) Schematics of the Co/Cu/Co film stack and the spin current in the structure. (b) In-plane hysteresis loops measured by VSM for the structures with different Co_2 thickness. (c) The measured effective magnetic anisotropy H_K^{eff} for the Co layers. (d) Schematic of a Hall-bar structure and configuration for the HLV measurement.

SOT induced by spin polarization with spin rotation (SR) symmetry [32]. The recent works have shown that the anomalous SOT with SR symmetry in $FM_1/NM/FM_2$ trilayers can be explained by the spin swapping effect [33] and the spin-orbit precession (SOP) effect [34–36]. In the spin swapping scenario, electrons flowing in the FM acquire a spin polarization along $\hat{m}$ (the unit vector of magnetization) and may scatter towards the NM layer. Once in the NM, these electrons experience spin swapping: upon scattering on spin-orbit coupled impurities, they experience a spin-orbit field oriented normal to the scattering plane [i.e., along $\hat{z} \times \hat{k}$] and about which their spin processes. Upon this reorientation, a spin current polarized along $\hat{m} \times (\hat{z} \times \hat{k})$ ($\hat{z}$ is the normal direction of the interface and $\hat{k}$ is the wave vector of conducting electrons along the opposite direction of the current) is produced. In the SOP scenario, as a charge current is applied in the FM_1 layers, owing to the strong exchange interaction, the spins are polarized along the magnetization direction of the FM_1 layer. However, when the spins reach the FM_1/NM and/or NM/FM_2 interfaces, they precess around the interfacial Rashba spin-orbit field $\hat{H}_R \propto \hat{z} \times \hat{k}$, thus producing a spin current with polarization along the $\hat{m} \times (\hat{z} \times \hat{k})$ direction. The spin current with $\hat{m} \times (\hat{z} \times \hat{k})$ polarization passes through the NM layer and exerts torque on the FM_2 layer (spin-detection layer), resulting in a SOT with SR symmetry. As illustrated in Fig. 1(a), if the FM_1 layer is out-of-plane magnetized ($\hat{m}//\hat{z}$), a spin current with spin polarization along the x direction ($\hat{\sigma}_x$) is injected into the FM_2 layer [34–36]. Conversely, if the FM_1 layer is magnetized along the in-plane current direction ($\hat{m}//\hat{x}$), a spin current with spin polarization along the z direction ($\hat{\sigma}_z$) is injected into the FM_2 layer [37]. This effect has been demonstrated theoretically and experimentally by several groups [32,34–38]. As discussed previously, the UMR effect normally coexists with the SOT effect in magnetic heterostructures. However, up to now, the reported UMR effect is associated with spin polarization induced by SHE and/or REE in NM/FM bilayers, and the UMR induced by spin polarization with SR symmetry is seldom studied.

In this work, we demonstrate the coexistence of SOT and UMR induced by spin polarization with SR symmetry in a Co/Cu/Co structure with crossed anisotropy. We measured the angular and field dependence of the harmonic signals in the structures by utilizing the second harmonic longitudinal voltage (HLV) method. It is found that, in addition to the ordinary USMR that is normally observed in NM/FM bilayers, an extra unidirectional harmonic signal is observed in the HLV measurement when sweeping the field along the x and z directions. We further demonstrate that the unidirectional harmonic signal consists of two major contributions, i.e., the dampinglike SOT harmonic signal, and the UMR originating from bulk and/or interface scattering to the spin polarization with SR symmetry.

II. EXPERIMENTAL DETAILS

In this work, the film stack of substrate/Ta(1)/Pt(3)/Co(1)/Cu(3)/Co(d_{Co})/Ta(3) was deposited on thermally oxidized Si wafers by magnetron sputtering with a base pressure prior to 2×10^{-7} Torr (the numbers in parentheses are the layer thicknesses in nm, and $d_{Co} = 2, 3, 4, 5, 6$ nm). The bottom and upper Ta layers served as buffer and capping layers, respectively. The 3-nm-thick Pt layer was used to induce perpendicular magnetic anisotropy (PMA) in the bottom Co layer. The 3-nm-thick Cu acted as a spacer layer to prevent interlayer exchange coupling and transport the spin current. For simplicity, the structures are denoted as $Co_1/Cu/Co_2$ (d_{Co}) in the following text, where Co_1 represents the bottom PMA Co layer and the Co_2 represents the upper in-plane Co layer. The hysteresis loops of the film stacks were measured by vibrating sample magnetometry (VSM), as shown in Fig. 1(b). We observed two completely different parts in the loops, which were from two Co layers with different anisotropy. We obtained the effective magnetic anisotropy field (H_K^{eff}) from the saturation field of the in-plane $m-H$ loops and out-of-plane anomalous Hall effect (AHE) curves for the Co_1 and Co_2 layers (see Supplemental Material S1 [39] for the details), respectively, as summarized in Fig. 1(c). After deposition, the film stacks were patterned into Hall bar devices ($l \times w = 200\,\mu m \times 10\,\mu m$) by standard photolithography and ion milling techniques, as shown in Fig. 1(d).

We measured the current-induced harmonic voltage in the system by the HLV technique. First, a large out-of-plane field ($H_z^{'} = \pm 15$ kOe) was applied to the devices to initialize the Co_1 magnetized along the $\pm z$ direction. Then the devices were rotated in the xy plane under a constant in-plane magnetic field (H_{ext}) in the range 100–1000 Oe, which was large enough to align the magnetization coherently, but small enough to keep the perpendicularly magnetized state in the Co_1 layer. Meanwhile, a sinusoidal ac current $I = I_0\sin(\omega t)$ with a frequency ($\omega/2\pi$) of 133 Hz was applied to the devices. The ac output voltage $V(t)$ was recorded by a high-accuracy data acquisition card (NI-4461). The first and second HLV signals, i.e., V^{ω} and $V^{2\omega}$, were simultaneously obtained by fast Fourier transformation (FFT) of $V(t)$ at each angle. The harmonic resistance was calculated by $R^{\omega} = \frac{V^{\omega}}{I_0}$ and $R^{2\omega} = \frac{dR}{dI}I_0 = 2\frac{V^{2\omega}}{I_0}$. In addition, the maximum current

amplitude (I_0) in the HLV measurements was much less than the threshold current of the SOT-induced switching in the Co_1 layer, thus its magnetization direction remains unchanged. Taking into account all kinds of MR effects in the structure, including the anisotropic MR (AMR) in the FM layers, the SMR in the FM/NM, and the GMR effect in the Co/Cu/Co structure (see Supplemental Material S2 [39] for the measured GMR curve and its thickness dependence), the theoretical angular dependence of the harmonic signal induced by SOT from $\hat{\sigma}_y$ and $\hat{\sigma}_x$ can be expressed as (see Appendix A for the theoretical derivation)

$$R_{\hat{\sigma}_y}^{2\omega}(\varphi) = \frac{(R_x - R_y)(H_{SH,FL+Oe})}{2H_{ext}}(\sin 3\varphi + \sin\varphi)$$
$$\mp \frac{\Delta R_{GMR}H_{SH,DL}}{-H_K^{eff} + H_{ext}}\cos\varphi, \tag{1}$$

$$R_{\hat{\sigma}_x}^{2\omega}(\varphi) = \pm \frac{(R_x - R_y)H_{SR,FL}}{2H_{ext}}(\cos 3\varphi - \cos\varphi)$$
$$+ \frac{\Delta R_{GMR}H_{SR,DL}}{-H_K^{eff} + H_{ext}}\sin\varphi. \tag{2}$$

We noted that, for the SOT induced by $\hat{\sigma}_y$, the fieldlike (FL) [dampinglike (DL)] harmonic term is independent (dependent) on the magnetization direction of the Co_1 layer, while the opposite is true for the SOT induced by $\hat{\sigma}_x$. This difference is easy to understand because the DL-SOT harmonic signal induced by spin polarization with SR symmetry is the result of the combined action of spin polarization and GMR effect. The polarities of both depend on the magnetization direction of the Co_1 layer.

Next, we consider the UMR terms induced by spin polarization with different directions. In the spin-dependent scattering mechanism scenario, UMR is proportional to the dot product of the magnetization vector and the spin polarization, and the amplitude of the current. For the specified Co/Cu/Co structures with crossed anisotropy in this work, taking into account the spin polarization with SH and SR symmetries, the total $R_{UMR}^{2\omega}$ can be written as (see Appendix B for details)

$$R_{UMR}^{2\omega} \propto \left(\theta_{Pt}^{SH}\sin\theta_1 + |\theta_{Ta}^{SH}|\right)I_0\sin\varphi$$
$$- \left(\theta_{Co1}^{SR} + \theta_{Co2}^{SR}\right)I_0\cos\theta_1\cos\varphi, \tag{3}$$

where θ_1 is the polar angle of the Co_1 layer and θ^{SH} and θ^{SR} indicate the charge to spin conversion efficiencies with SH and SR symmetries. For the in-plane rotation sweeping under a small field, $\sin\theta_1 \approx 0$ and $\cos\theta_1 \approx \pm 1$, then we have

$$R_{UMR}^{2\omega} \propto \alpha\sin\varphi \pm \beta\cos\varphi, \tag{4}$$

where α and β are coefficients proportional to the current amplitude. Therefore, the total harmonic resistance from HLV measurement is the sum of Eqs. (1), (2), and (4).

III. RESULTS AND DISCUSSION

Figures 2(a) and 2(b) show the angular dependence of the harmonic resistance obtained for the $Co_1(1)/Cu(3)/Co_2(6)$ sample with $H_{ext} = 400$ Oe and $I_0 = 11.48$ mA. The R^ω term includes the AMR from the Co_2 layer and the possible SMR

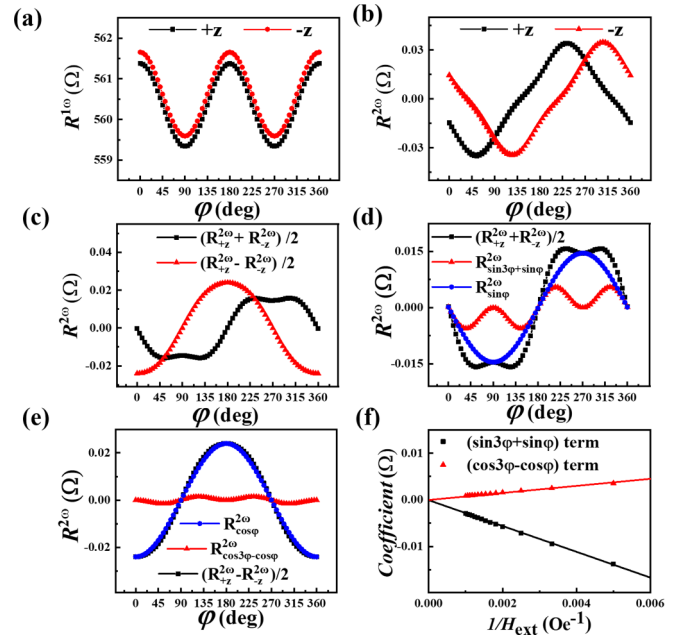FIG. 2. The results of the HLV measurement for the $Co(1)/Cu(3)/Co(6)$ structures. (a) The $R^\omega(\varphi)$ and (b) the $R^{2\omega}(\varphi)$ with $+z$ and $-z$ states for the $Co_1(1)/Cu(3)/Co(6)$ sample. (c) The obtained $(R_{+z}^{2\omega} \pm R_{-z}^{2\omega})/2$ from (b). The theoretical fitting to the (d) $(R_{+z}^{2\omega} + R_{-z}^{2\omega})/2$ and (e) $(R_{+z}^{2\omega} - R_{-z}^{2\omega})/2$ terms. (f) Coefficients of the $(\sin 3\varphi + \sin\varphi)$ and $(\cos 3\varphi - \cos\varphi)$ terms as a function of $1/H_{ext}$.

originating from Co_2/Ta bilayer [40,41]. It should be noted that although the typical Co/Cu/Co structure possesses a large GMR effect, the relative orientation of two Co layers keep constant during the in-plane rotation, therefore the GMR effect is not included in the $R^\omega - \varphi$ curves. The general angular dependence of the R^ω term can be expressed as

$$R^\omega(\varphi) = R_y + (R_x - R_y)\cos^2\varphi, \tag{5}$$

where $R_x(R_y)$ is the longitudinal resistance when the magnetization is saturated along the $x(y)$ direction. Figure 2(b) shows the angular dependence of $R^{2\omega}$ with the Co_1 layer magnetized along the $+z$ [$R_{+z}^{2\omega}(\varphi)$] and $-z$ [$R_{-z}^{2\omega}(\varphi)$] direction. Apparently, the difference of $R^{2\omega}$ between the $+z$ and $-z$ states confirmed the effect of the bottom Co_1 magnetization. To analyze the signals, we calculated $(R_{+z}^{2\omega} + R_{-z}^{2\omega})/2$ and $(R_{+z}^{2\omega} - R_{-z}^{2\omega})/2$ terms and plotted them in Fig. 2(c). We found that the $(R_{+z}^{2\omega} + R_{-z}^{2\omega})/2$ term consists of the $(\sin 3\varphi + \sin\varphi)$ term and the $\sin\varphi$ term, while the $(R_{+z}^{2\omega} - R_{-z}^{2\omega})/2$ terms consists of the $(\cos 3\varphi - \cos\varphi)$ and $\cos\varphi$ terms, which correspond to the four terms in Eqs. (1)–(3), as shown in Figs. 2(d) and 2(e). Compared with the equations, it can be found that the $(\sin 3\varphi + \sin\varphi)$ term is derived from the transverse effective field (including the $\hat{\sigma}_y$-induced FL-SOT effective field and the current-induced Oersted field), and the $(\cos 3\varphi - \cos\varphi)$ term is the pure contribution from the $\hat{\sigma}_x$-induced FL-SOT. Figure 2(f) shows the linear fitting to the coefficient of the $(\cos 3\varphi - \cos\varphi)$ and $(\sin 3\varphi + \sin\varphi)$ as a function of $1/H_{ext}$, from which we obtained the $\hat{\sigma}_x$-induced FL-SOT effective field ($H_{SR,FL}$) and the ordinary transverse effective field [i.e., the sum of the $\hat{\sigma}_y$-induced FL-SOT effective field ($H_{SH,FL}$)
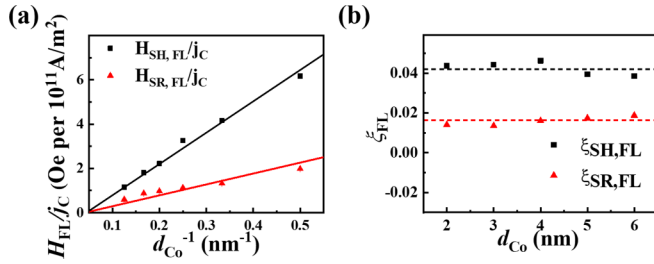
FIG. 3. The Co_2 thickness dependence of the FL-SOT effective fields per current density and FL-SOT efficiency. (a) The linear fitting to the FL-SOT effective fields plotted with the inverse of the Co thickness (d_{Co}^{-1}). (b) The calculated FL-SOT efficiency of $\hat{\sigma}_x$ ($\xi_{SR,FL}$) and $\hat{\sigma}_y$ ($\xi_{SH,FL}$) for the samples with different d_{Co}.

and the current-induced Oersted field (H_{Oe})], respectively. We obtained $H_{SH,FL}$ by subtracting H_{Oe} from the total transverse field, in which H_{Oe} was estimated by a simple parallel resistor model.

Finally, we carried out the same measurement for all the samples, and obtained $H_{SR,FL}$ and $H_{SH,FL}$ per unit current density, as plotted in Fig. 3(a), which follows the $1/d_{Co}$ law roughly. We calculated the FL-SOT efficiency of spin polarization with SR symmetry ($\xi_{SR,FL}$) and SH symmetry ($\xi_{SH,FL}$) by $\xi_{FL} = (2e/\hbar)(M_S d_{Co} H_{FL}/j_C)$, and obtained $\xi_{SR,FL} = 0.017$ and $\xi_{SH,FL} = 0.041$, as shown in Fig. 3(b). These results are basically consistent with that obtained from the harmonic Hall voltage (HHV) measurements (see Supplemental Material S3 [39]).

The $\sin\varphi$ ($\cos\varphi$) harmonic term corresponds to a unidirectional signal along the $y(x)$ direction. To further investigate their origins, we measured $R^{2\omega}$ as a function of the external magnetic field applied along the different directions, as shown in Fig. 4. For the $R^{2\omega} - H_x$ and $R^{2\omega} - H_y$ curves, the samples were initially magnetized along the $\pm z$ direction before measurements. It is found that the polarity of $R^{2\omega} - H_x$ [Fig. 4(a)] depends on the magnetization states of the Co_1 layer, but the polarity of $R^{2\omega} - H_y$ [Fig. 4(b)] is independent of that. Similar to the USMR curves observed in NM/FM bilayer, two spikes were observed near the zero field in the $R^{2\omega} - H_y$ curves, which probably originated from the electron-magnon scattering effect or the nonuniform magnetization of the Co layer. The unidirectional harmonic signal is also observed as the field is sweeping along the z direction [Fig. 4(c)]. In this case, an auxiliary in-plane field along the x direction ($H_x = \pm 100$ Oe) must be applied to align the magnetization of the Co_2 layer. The unidirectional harmonic signal has the same magnitude as that obtained from the $R^{2\omega} - H_x$ curve, and it disappears when the in-plane field (H_{in}) turns to the y direction with a $\cos\varphi$ dependence, as shown in Fig. 4(f) (see Supplemental Material S4 [39] for the detailed $R^{2\omega} - H_z$ curves measured with different H_{in} direction). We will see that, from the viewpoint of both mechanisms, the measured unidirectional harmonic signal with the field along the x direction is completely equivalent to that along the z direction (with $\hat{m}_{Co_2}//\hat{y}$).

Next, we discuss the origins of the observed unidirectional harmonic signal. From Eqs. (1) and (2), it can be found that the DL-SOT harmonic signals induced by the spin current
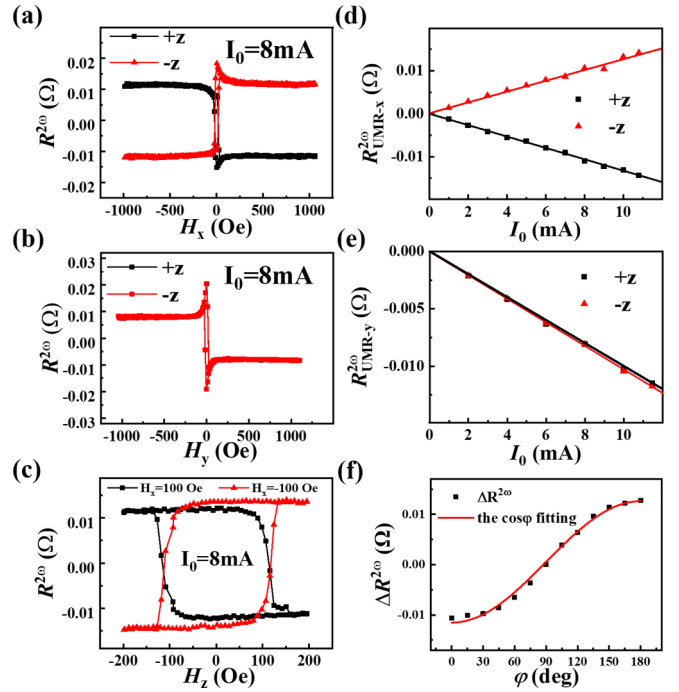

FIG. 4. Field and current dependence of the unidirectional harmonic signal obtained by a field sweep measurement. (a)–(c) The measured $R^{2\omega} - H$ curves with the field applied along the x, y, and z directions with $I_0 = 8$ mA for the $Co(1)/Cu(3)/Co(6)$ sample. A constant field is applied along the x direction ($H_x = \pm 100$ Oe) for the measurement of the $R^{2\omega} - H_z$ curves in (c). (d),(e) The linear fitting to the current amplitude dependence of the unidirectional harmonic signal. (f) The in-plane field azimuth angle dependence of the unidirectional harmonic signal measured by field sweep along the z direction ($\varphi = 0$ corresponds to the in-plane field applied along the $+x$ direction).

of $\hat{\sigma}_y$ and $\hat{\sigma}_x$ exhibit $\cos\varphi$ and $\sin\varphi$ angular dependence, respectively. Besides, as we known, the magnetothermal signal induced by perpendicular temperature gradients ($R^{2\omega}_{xx,\nabla T}$) [42–49] (see Supplemental Material S5 [39]) and the USMR effect induced by $\hat{\sigma}_y$ ($R^{2\omega}_{USMR}$) in the NM/FM bilayers also show $\sin\varphi$ dependence. In the same way, similar to the USMR mechanism, the accumulation of $\hat{\sigma}_x$ in the in-plane Co_2 layer or at its interface will also contribute a UMR with $\cos\varphi$ dependence [Eq. (3)]. We clarify that although the in-plane temperature gradients caused by the lateral asymmetry may exist in our sample, they cannot give rise to the harmonic signal with $\sin\varphi$ or $\cos\varphi$ dependence. In summary, the measured unidirectional harmonic signal with the field sweeping along the y direction (the $\sin\varphi$ term) includes three origins: the DL-SOT harmonic signal induced by $\hat{\sigma}_x$ ($R^{2\omega}_{DL(\hat{\sigma}_x)}$), the UMR induced by $\hat{\sigma}_y$ (USMR), and the harmonic magnetothermal signal induced by ∇T ($R^{2\omega}_{xx,\nabla T}$), while the measured unidirectional harmonic signal with the field sweeping along the x direction (the $\cos\varphi$ term) includes two origins: the DL-SOT harmonic signal induced by $\hat{\sigma}_y$ ($R^{2\omega}_{DL(\hat{\sigma}_y)}$) and the UMR induced by the spin polarization with SR symmetry (SR-UMR). We need to emphasize that the unidirectional harmonic signal obtained from the $R^{2\omega} - H_z$ (with $\hat{m}_{Co_2}//\hat{x}$) measurement is equivalent to that from the $R^{2\omega} - H_x$ curve (with $\hat{m}_{Co_1}//\hat{z}$).
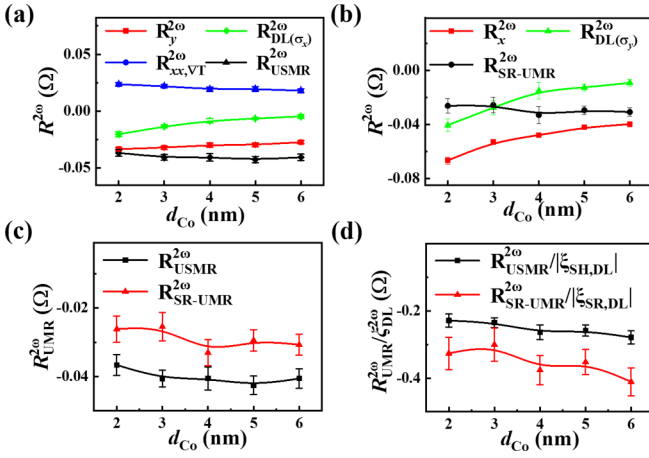
FIG. 5. The Co_2 layer thickness dependence of the USMR, SR-UMR, and the ratios with the corresponding DL-SOT efficiencies. (a) $R_y^{2\omega}$, $R_{xx,\nabla T}^{2\omega}$, $R_{DL(\hat{\sigma}_x)}^{2\omega}$, and $R_{USMR}^{2\omega}$ as a function of d_{Co}. (b) $R_x^{2\omega}$, $R_{DL(\hat{\sigma}_y)}^{2\omega}$, and $R_{SR-UMR}^{2\omega}$ as a function of d_{Co}. (c) Comparison of the $R_{USMR}^{2\omega}$ and $R_{SR-UMR}^{2\omega}$ as a function of d_{Co}. (d) Comparison of $R_{USMR}^{2\omega}/|\xi_{SH,DL}^{2\omega}|$ and $R_{SR-UMR}^{2\omega}/|\xi_{SR,DL}^{2\omega}|$ as a function of d_{Co}.

In the spin-dependent scattering SR-UMR scenario, besides the accumulation of $\hat{\sigma}_x$ in the in-plane Co_2 layer or at its interface, the spin current with $\hat{\sigma}_z$ polarization induced by the SR effect from the Co_2 layer may accumulate at the bottom Cu/Co_1 interface, resulting in an extra UMR. No matter which Co layer is reversed, the UMR from both interfaces change its sign, therefore they are included in the $R^{2\omega} - H_z$ and $R^{2\omega} - H_x$ curves. From the SOT viewpoint, we noted that the unidirectional harmonic signal [the second term of Eq. (2)] induced by DL-SOT from spin polarization with SR symmetry depends on the polarity of the GMR curve and the azimuth angle; as a result, the reversal of either Co_1 or Co_2 layer results in the reversal of the unidirectional harmonic signal. Therefore, the measured unidirectional harmonic signal from Figs. 4(a) and 4(c) are completely equivalent.

Finally, we separate the different contributions of the measured unidirectional harmonic signals. To avoid the influence of the observed spikes at low field, we focus on the constant unidirectional harmonic signal observed at $H_{x(y)} > 200$ Oe. Among the different origins of the them, the $R_{xx,\nabla T}^{2\omega}$ term can be obtained by using the relationship $R_{xx,\nabla T}^{2\omega} = \frac{l}{w}R_{H,\nabla T}^{2\omega}$ ($R_{H,\nabla T}^{2\omega}$ is the magnetothermal term measured from HHV, l and w are the length and width of the Hall-bar device) [29]. In addition, we estimate the values of $R_{DL(\hat{\sigma}_y)}^{2\omega}$ and $R_{DL(\hat{\sigma}_x)}^{2\omega}$ according to Eqs. (1) and (2), respectively, by using the DL-SOT effective field values obtained from HHV measurement, the ΔR_{GMR} and H_K^{eff} values. Then, by subtracting the $R_{DL(\hat{\sigma}_x)}^{2\omega}$ term and the $R_{xx,\nabla T}^{2\omega}$ terms from the unidirectional harmonic signal measured with the field applied along the y direction (i.e., the $\sin\varphi$ term), we obtain the value of USMR, as shown in Fig. 5(a). Similarly, the SR-UMR term is obtained by subtracting the DL-SOT harmonic signal $R_{DL(\hat{\sigma}_y)}^{2\omega}$ from the unidirectional harmonic signal measured with the field along the x or z directions (i.e., the $\cos\varphi$ term), as shown in Fig. 5(b). We noted that the $R_{USMR}^{2\omega}$ and $R_{SR-UMR}^{2\omega}$ were of the same order of magnitude and exhibited a similar variation

trend with increasing d_{Co} [Fig. 5(c)]. The microscopic mechanism of SR-UMR is similar to that of $\hat{\sigma}_y$-induced USMR in NM/FM bilayers. The spin accumulation in the FM layer (or at the NM/FM interface) modulates the conductivity of the FM layer (or interfacial spin transport) by spin-dependent scattering, resulting in the spin polarization-related UMR effect. For the $\hat{m}_{Co_1} // + \hat{z}$ state, the SR-UMR is negative, which corresponds to the low-resistance state when the Co_2 layer is magnetized along the $+x$ direction, suggesting that the spin polarization of SR symmetry is along the $+x$ direction for the $\hat{m}_{Co_1} // + \hat{z}$ state. This is in agreement with the positive FL-SOT effective field of SR symmetry when the Co_1 layer is magnetized along $+z$ direction. In addition, because both the DL-SOT and the UMR are related to the magnitude of spin current, we compared the ratio of USMR (SR-UMR) and the corresponding DL-SOT efficiency as a function of d_{Co}, as shown in Fig. 5(d). We found that the spin polarization with SH symmetry and SR symmetry gave rise to a different $R_{UMR}^{2\omega}/|\xi_{DL}|$. We argue that this difference resulted for the following two reasons: (1) the measured SOT from spin polarization with SR symmetry only includes the torque exerting on the Co_2 layer, while the SR-UMR includes the contribution from both interfaces; (2) even only comparing the effect of $\hat{\sigma}_x$ and $\hat{\sigma}_y$, spin accumulation is induced at a different interface: $\hat{\sigma}_x$ originates from the bottom Co_1 layer and/or its interface, and accumulates at the Cu/Co_2 interface, while $\hat{\sigma}_y$ mostly originates from the SHE in the bulk Ta layer and the Rashba effect at Cu/Co_2 interfaces. Different interface properties will result in a different ratio of USMR (SR-UMR) and SOT efficiency.

IV. CONCLUSIONS

In summary, we demonstrated that besides the harmonic signal induced by spin polarization with SH symmetry, the SOT and UMR from spin polarization with SR symmetry coexist in the Co/Cu/Co heterostructures with crossed anisotropy. Among them, the FL-SOT and UMR harmonic signal induced by spin polarization with SR symmetry is dependent on the magnetization state of the PMA Co layer; while the DL-SOT harmonic signal is independent of that due to the combined effect of the SR property and GMR curve. By combining the SOT effective fields from harmonic Hall voltage measurement, we successfully obtained the pure USMR induced by spin polarization with SH symmetry, and the SR-UMR induced by spin polarization with SR symmetry. The discovery of this SR-UMR provides another solid evidence for the existence of spin polarization with SR symmetry in FM/NM/FM structures and is of importance for its possible application in spintronic devices.

APPENDIX A: THEORETICAL DERIVATION OF THE HARMONIC LONGITUDINAL VOLTAGE SIGNAL INDUCED BY DIEFFERENT SPIN POLARIZATION

For the $FM_1/NM/FM_2$ trilayer structure, the ordinary spin current with spin polarization along the y direction ($\hat{\sigma}_y$) may exert spin torques on the FM_2 layer, resulting in harmonic longitudinal voltage signals. In addition, if the FM_1 layer is out-of-plane magnetized ($\hat{m}//\hat{z}$), a spin current with spin polarization along the x direction $\hat{\sigma}_x$ will be induced by the spin-orbit precession (SOP) effect at the FM_1/NM and/or NM/FM_2 interfaces, which cause an external harmonic longitudinal voltage (HLV) signal. In this part, we deduct the theoretical formulas for the harmonic longitudinal resistance induced by $\hat{\sigma}_x$ and $\hat{\sigma}_y$ spin polarization based on a macrospin model.

When a charge current flows along $+\hat{x}$ direction, the current-induced effective field $\Delta H_{x,y,z}$ (including the SOT effective fields and current-induced Oersted field) can change the direction of the equilibrium magnetization $\vec{M}(\theta, \varphi)$ with a modulation amplitude of $(\Delta\theta, \Delta\varphi)$. Considering a FM layer with effective perpendicular magnetic anisotropy field of H_K^{eff}, $(\Delta\theta, \Delta\varphi)$ can be expressed as [50,51]

$$\Delta\theta = \frac{\cos\theta(\Delta H_x\cos\varphi + \Delta H_y\sin\varphi) - \sin\theta\Delta H_z}{H_K^{\text{eff}}\cos2\theta + H_{\text{ext}}\cos(\theta_H - \theta)}, \quad (A1)$$

$$\Delta\varphi = \frac{-\Delta H_x\sin\varphi_H + \Delta H_y\cos\varphi_H}{H_{\text{ext}}\sin\theta_H}, \quad (A2)$$

where θ_H, φ_H represents the polar and azimuthal angles of the external magnetic field. According to the SHE and SOP theory, the corresponding SOT effective fields can be expressed as (a) $\vec{H}_{\text{SH,DL}} \propto \hat{m}_{\text{IN}} \times (\hat{z} \times \hat{J}_C)$; (b) $\vec{H}_{\text{SH,FL}} \propto \hat{z} \times \hat{J}_C$; (c) $\vec{H}_{\text{SR,DL}} \propto \hat{m}_{\text{IN}} \times [\hat{m} \times (\hat{z} \times \hat{J}_C)]$; (d) $\vec{H}_{\text{SR,FL}} \propto \hat{m} \times (\hat{z} \times \hat{J}_C)$. $\hat{m}_{\text{IN}}$ represents the unit vector magnetization of the Co_2 layer, and $\hat{m}$ represents the unit vector magnetization of the bottom Co_1 layer. It is obvious that $\vec{H}_{\text{SR,DL}}$ and $\vec{H}_{\text{SR,FL}}$ are related to the magnetization direction of the Co_1 layer. Suppose the Co_1 layer is magnetized along the $+\hat{z}$ direction: the effective field of SOT with SH symmetry ($H_{\text{SH,DL}}$, $H_{\text{SH,FL}}$) and spin rotation symmetry ($H_{\text{SR,DL}}$, $H_{\text{SR,FL}}$) can be written as

$$\Delta\vec{H}_{\hat{\sigma}_y} = (\Delta H_x, \Delta H_y, \Delta H_z)$$
$$= (0, H_{\text{SH,FL}} + H_{\text{Oe}}, H_{\text{SH,DL}}\cos\varphi), \quad (A3)$$

$$\Delta\vec{H}_{\hat{\sigma}_x} = (\Delta H_x, \Delta H_y, \Delta H_z) = (\pm H_{\text{SR,FL}}, 0, \mp H_{\text{SR,DL}}\sin\varphi). \quad (A4)$$

Considering that the Co_2 layer has negligible in-plane anisotropy, as the magnetization rotates in the xy plane under an external field, we have $\theta_H = \theta = 90°$, $\varphi_H = \varphi$, then

$\Delta\theta$ and $\Delta\varphi$ (subscript means generated by $\hat{\sigma}_y$ or $\hat{\sigma}_x$) can be written as

$$\Delta\theta_{\hat{\sigma}_y} = \frac{-H_{\text{SH,DL}}\cos\varphi}{-H_K^{\text{eff}} + H_{\text{ext}}}, \Delta\theta_{\hat{\sigma}_x} = \frac{\pm H_{\text{SR,DL}}\sin\varphi}{-H_K^{\text{eff}} + H_{\text{ext}}}, \quad (A5)$$

$$\Delta\varphi_{\hat{\sigma}_y} = \frac{H_{\text{SH,FL}}\cos\varphi}{H_{\text{ext}}}, \Delta\varphi_{\hat{\sigma}_x} = \frac{\mp H_{\text{SR,FL}}\sin\varphi}{H_{\text{ext}}}. \quad (A6)$$

Then we consider the HLV measurements. When a sinusoidal current ($I = I_0\sin\omega t$) is applied, the magnetization oscillates synchronously with the current polarity. Taking into account the resistance change resulting from the current-induced effective fields, a nonlinear resistance term should be introduced, i.e.,

$$R = R_0 + R(I) = R_0 + \frac{dR}{dI}I. \quad (A7)$$

When a sinusoidal current ($I = I_0\sin\omega t$) is applied, we have

$$V(t) = R(t)I(t) = \left(R_0 + \frac{dR}{dI}I_0\sin\omega t\right)I_0\sin\omega t$$
$$= V^0 + V^\omega\sin\omega t + V^{2\omega}\cos2\omega t, \quad (A8)$$

where

$$V^\omega = R^\omega I_0, V^{2\omega} = -\frac{1}{2}R^{2\omega}I_0; \quad (A9)$$

R^ω ($R^{2\omega}$) represents the first (second) harmonic longitudinal resistance.

Considering the AMR, GMR, and SMR effect in the structure with cross anisotropy, the longitudinal resistance R can be written by

$$R = R_z + (R_x - R_z)(\sin\theta\cos\varphi)^2 + (R_y - R_z)(\sin\theta\sin\varphi)^2$$
$$+ \Delta R_{\text{GMR}}\cos(\theta_1 - \theta), \quad (A10)$$

where ΔR_{GMR} represents the resistance difference between parallel and orthogonal configuration of the two Co layers, and θ represents the polar angle of the Co_2 layer. θ_1 represents the polar angle of the Co_1 layer, which is nearly 0 or 180° in the case of weak in-plane field applied, corresponding to the Co_1 layer magnetized along the $+z$ and $-z$ directions, respectively.

As the magnetization rotates in the xy plane under a weak in-plane field ($\theta \approx 90°$), by performing Taylor expansion to (A10), the expression of R can be written as

$$R = R_x\cos^2\varphi + R_y\sin^2\varphi - (R_x - R_y)\sin2\varphi\Delta\varphi \mp \Delta R_{\text{GMR}}\Delta\theta. \quad (A11)$$

The last two terms in Eq. (A11) represent the resistance oscillation induced by current-induced effective field, which corresponds to the second harmonic resistance, i.e.,

$$R^{2\omega} = (R_x - R_y)\sin2\varphi\Delta\varphi \mp \Delta R_{\text{GMR}}\Delta\theta. \quad (A12)$$

Substituting Eq. (A5) and Eq. (A6) into Eq. (A12), we obtained the angular dependence of the second harmonic

longitudinal resistance $R_{\hat{\sigma}_x}^{2\omega}(\varphi)$ and $R_{\hat{\sigma}_y}^{2\omega}(\varphi)$ induced by $\hat{\sigma}_x$ and $\hat{\sigma}_y$, respectively, expressed as

$$R_{\hat{\sigma}_x}^{2\omega}(\varphi) = \pm \frac{(R_x - R_y)H_{\mathrm{SR,FL}}(\cos 3\varphi - \cos\varphi)}{2H_{\mathrm{ext}}}$$
$$+ \frac{\Delta R_{\mathrm{GMR}}H_{\mathrm{SR,DL}}}{-H_K^{\mathrm{eff}} + H_{\mathrm{ext}}}\sin\varphi, \qquad (\mathrm{A}13)$$

$$R_{\hat{\sigma}_y}^{2\omega}(\varphi) = \frac{(R_x - R_y)H_{\mathrm{SH,FL+Oe}}(\sin 3\varphi + \sin\varphi)}{2H_{\mathrm{ext}}}$$
$$\mp \frac{\Delta R_{\mathrm{GMR}}H_{\mathrm{SH,DL}}}{-H_K^{\mathrm{eff}} + H_{\mathrm{ext}}}\cos\varphi. \qquad (\mathrm{A}14)$$

APPENDIX B: THEORETICAL AUGULAR DEPENDENCE OF THE UMR SIGNAL INDUCED BY DIFFERENT SPIN PORLARIZATION

For the $\mathrm{Co_1/Cu/Co_2}$ structure with two FM layers, according to the coordinate definition, the unit vector of the magnetization of two Co layers can be written as

$$\hat{m}_{\mathrm{Co1}} = (\sin\theta_1\cos\varphi, \sin\theta_1\sin\varphi, \cos\theta_1), \qquad (\mathrm{B}1)$$

$$\hat{m}_{\mathrm{Co2}} = (\cos\varphi, \sin\varphi, 0). \qquad (\mathrm{B}2)$$

The spin polarization with SR symmetry produced from the $\mathrm{Co_1}$ ($\sigma_{\mathrm{Co1}}^{\mathrm{SR}}$)and the $\mathrm{Co_2}$ ($\sigma_{\mathrm{Co2}}^{\mathrm{SR}}$) layers can be expressed as

$$\sigma_{\mathrm{Co1}}^{\mathrm{SR}} \propto \hat{m}_{\mathrm{Co1}} \times (\hat{z} \times \hat{k}) = (-\cos\theta_1, 0, \sin\theta_1\cos\varphi), \qquad (\mathrm{B}3)$$

$$\sigma_{\mathrm{Co2}}^{\mathrm{SR}} \propto \hat{m}_{\mathrm{Co2}} \times (\hat{z} \times \hat{k}) = (0, 0, -\cos\varphi), \qquad (\mathrm{B}4)$$

where $\hat{z}$ represent the normal direction of the interface and $\hat{k}$ is the wave vector of conducting electrons along the opposite direction of the current. In spin-dependent scattering mechanism scenario, UMR is proportional to the dot product of magnetization vector and spin polarization. Therefore, the UMR induced by spin polarization with SR symmetry is

$$R_{\mathrm{SR-UMR}}^{2\omega} \propto -\left(\theta_{\mathrm{Co1}}^{\mathrm{SR}} + \theta_{\mathrm{Co2}}^{\mathrm{SR}}\right)I_0\cos\theta_1\cos\varphi. \qquad (\mathrm{B}5)$$

Including the USMR terms induced by the spin current from the adjacent Ta and Pt layers, we obtain the total UMR expression,

$$R_{\mathrm{UMR}}^{2\omega} \propto \left(\theta_{\mathrm{Pt}}^{\mathrm{SH}}\sin\theta_1 + \left|\theta_{\mathrm{Ta}}^{\mathrm{SH}}\right|\right)I_0\sin\varphi$$
$$- \left(\theta_{\mathrm{Co1}}^{\mathrm{SR}} + \theta_{\mathrm{Co2}}^{\mathrm{SR}}\right)I_0\cos\theta_1\cos\varphi, \qquad (\mathrm{B}6)$$

where θ_1 is the polar angle of the $\mathrm{Co_1}$ layer and θ^{SH} and θ^{SR} indicate the effective charge to spin conversion efficiencies of SH and SR symmetries.

[1] J. C. Slonczewski, J. Magn. Magn. Mater. **159**, L1 (1996).
[2] L. Berger, Phys. Rev. B **54**, 9353 (1996).
[3] I. Žutić, F. Jaroslav, and S. Das Sarma, Rev. Mod. Phys. **76**, 323 (2004).
[4] L. Liu, O. J. Lee, T. J. Gudmundsen, D. C. Ralph, and R. A. Buhrman, Phys. Rev. Lett. **109**, 096602 (2012).
[5] A. Manchon, J. Zelezny, I. M. Miron, T. Jungwirth, J. Sinova, A. Thiaville, K. Garello, and P. Gambardella, Rev. Mod. Phys. **91**, 035004 (2019).
[6] L. Zhu, D. C. Ralph, and R. A. Buhrman, Phys. Rev. Lett. **122**, 077201 (2019).
[7] M. Aoki, E. Shigematsu, M. Matsushima, R. Ohshima, S. Honda, T. Shinjo, M. Shiraishi, and Y. Ando, Phys. Rev. B **102**, 174442 (2020).
[8] Y. Hibino, T. Taniguchi, K. Yakushiji, A. Fukushima, H. Kubota, and S. Yuasa, Phys. Rev. Appl. **14**, 064056 (2020).
[9] M.-H. Nguyen, D. C. Ralph, and R. A. Buhrman, Phys. Rev. Lett. **116**, 126601 (2016).
[10] J. Kim, J. Sinha, M. Hayashi, M. Yamanouchi, S. Fukami, T. Suzuki, S. Mitani, and H. Ohno, Nat. Mater. **12**, 240 (2013).
[11] J. Sinova, S. O. Valenzuela, J. Wunderlich, C. H. Back, and T. Jungwirth, Rev. Mod. Phys. **87**, 1213 (2015).
[12] J. E. Hirsch, Phys. Rev. Lett. **83**, 1834 (1999).
[13] O. Krupin, G. Bihlmayer, K. Starke, S. Gorovikov, J. E. Prieto, K. Döbrich, S. Blügel, and G. Kaindl, Phys. Rev. B **71**, 201403(R) (2005).
[14] I. M. Miron, G. Gaudin, S. Auffret, B. Rodmacq, A. Schuhl, S. Pizzini, J. Vogel, and P. Gambardella, Nat. Mater. **9**, 230 (2010).
[15] H. Nakayama, Y. Kanno, H. An, T. Tashiro, S. Haku, A. Nomura, and K. Ando, Phys. Rev. Lett. **117**, 116602 (2016).

[16] Y. Lv, J. Kally, D. Zhang, J. S. Lee, M. Jamali, N. Samarth, and J. P. Wang, Nat. Commun. **9**, 111 (2018).
[17] D. Hsieh, Y. Xia, D. Qian, L. Wray, J. H. Dil, F. Meier, J. Osterwalder, L. Patthey, J. G. Checkelsky, N. P. Ong, A. V. Fedorov, H. Lin, A. Bansil, D. Grauer, Y. S. Hor, R. J. Cava, and M. Z. Hasan, Nature (London) **460**, 1101 (2009).
[18] X.-L. Qi and S.-C. Zhang, Rev. Mod. Phys. **83**, 1057 (2011).
[19] M. Neupane, A. Richardella, J. Sanchez-Barriga, S. Y. Xu, N. Alidoust, I. Belopolski, C. Liu, G. Bian, D. Zhang, D. Marchenko, A. Varykhalov, O. Rader, M. Leandersson, T. Balasubramanian, T.-R. Chang, H.-T. Jeng, S. Basak, H. Lin, A. Bansil, N. Samarth, and M. Z. Hasan, Nat. Commun. **5**, 3841 (2014).
[20] T. Taniguchi, J. Grollier, and M. D. Stiles, Phys. Rev. Appl. **3**, 044001 (2015).
[21] J. D. Gibbons, D. MacNeill, R. A. Buhrman, and D. C. Ralph, Phys. Rev. Appl. **9**, 064033 (2018).
[22] W. Wang, T. Wang, V. P. Amin, Y. Wang, A. Radhakrishnan, A. Davidson, S. R. Allen, T. J. Silva, H. Ohldag, D. Balzar, B. L. Zink, P. M. Haney, J. Q. Xiao, D. G. Cahill, V. O. Lorenz, and X. Fan, Nat. Nanotechnol. **14**, 819 (2019).
[23] R. E. Camley and J. Barnaś, Phys. Rev. Lett. **63**, 664 (1989).
[24] W. P. Pratt, Jr., S.-F. Lee, J. M. Slaughter, R. Loloee, P. A. Schroeder, and J. Bass, Phys. Rev. Lett. **66**, 3060 (1991).
[25] S. S. P. Parkin, C. Kaiser, A. Panchula, P. M. Rice, B. Hughes, M. Samant, and S. H. Yang, Nat. Mater. **3**, 862 (2004).
[26] Y.-T. Chen, S. Takahashi, H. Nakayama, M. Althammer, S. T. B. Goennenwein, E. Saitoh, and G. E. W. Bauer, Phys. Rev. B **87**, 144411 (2013).
[27] H. Nakayama, M. Althammer, Y. T. Chen, K. Uchida, Y. Kajiwara, D. Kikuchi, T. Ohtani, S. Geprags, M. Opel,

S. Takahashi, R. Gross, G. E. W. Bauer, S. T. B. Goennenwein, and E. Saitoh, Phys. Rev. Lett. **110**, 206601 (2013).

[28] S. Cho, S. C. Baek, K. D. Lee, Y. Jo, and B. G. Park, Sci. Rep. **5**, 14668 (2015).

[29] C. O. Avci, K. Garello, A. Ghosh, M. Gabureac, S. F. Alvarado, and P. Gambardella, Nat. Phys. **11**, 570 (2015).

[30] C. O. Avci, K. Garello, J. Mendil, A. Ghosh, N. Blasakis, M. Gabureac, M. Trassin, M. Fiebig, and P. Gambardella, Appl. Phys. Lett. **107**, 192405 (2015).

[31] C. O. Avci, J. Mendil, G. S. D. Beach, and P. Gambardella, Phys. Rev. Lett. **121**, 087207 (2018).

[32] A. M. Humpries, T. Wang, E. R. J. Edwards, S. R. Allen, J. M. Shaw, H. T. Nembach, J. Q. Xiao, T. J. Silva, and X. Fan, Nat. Commun. **8**, 911 (2017).

[33] H. B. M. Saidaoui and A. Manchon, Phys. Rev. Lett. **117**, 036601 (2016).

[34] Y. Hibino, K. Hasegawa, T. Koyama, and D. Chiba, APL Mater. **8**, 041110 (2020).

[35] Y. Hibino, T. Moriyama, K. Hasegawa, T. Koyama, T. Ono, and D. Chiba, Appl. Phys. Express **13**, 083001 (2020).

[36] T. Wang, S. Lendinez, M. B. Jungfleisch, J. Kolodzey, J. Q. Xiao, and X. Fan, Appl. Phys. Lett. **116**, 012404 (2020).

[37] S. C. Baek, V. P. Amin, Y.-W. Oh, G. Go, S.-J. Lee, G.-H. Lee, K.-J. Kim, M. D. Stiles, B.-G. Park, and K.-J. Lee, Nat. Mater. **17**, 509 (2018).

[38] Y. Hibino, K. Yakushiji, A. Fukushima, H. Kubota, and S. Yuasa, Phys. Rev. B **101**, 174441 (2020).

[39] See Supplemental Material at http://link.aps.org/supplemental/10.1103/PhysRevB.106.094422 for detailed information on the effective anisotropic field, typical GMR curve, harmonic Hall measurement, curves with different directions of in-plane field, and analysis of the magnetothermal harmonic signals.

[40] A. Kobs, S. Hesse, W. Kreuzpaintner, G. Winkler, D. Lott, P. Weinberger, A. Schreyer, and H. P. Oepen, Phys. Rev. Lett. **106**, 217207 (2011).

[41] M. Kawaguchi, D. Towa, Y.-C. Lau, S. Takahashi, and M. Hayashi, Appl. Phys. Lett. **112**, 202405 (2018).

[42] H. Wu, X. Wang, L. Huang, J. Y. Qin, C. Fang, X. Zhang, C. H. Wan, and X. F. Han, J. Magn. Magn. Mater. **441**, 149 (2017).

[43] S. Tu, J. Hu, G. Yu, H. Yu, C. Liu, F. Heimbach, X. Wang, J. Zhang, Y. Zhang, A. Hamzić, K. L. Wang, W. Zhao, and J.-P. Ansermet, Appl. Phys. Lett. **111**, 222401 (2017).

[44] S. M. Rezende, R. L. Rodríguez-Suárez, R. O. Cunha, A. R. Rodrigues, F. L. A. Machado, G. A. Fonseca Guerra, J. C. Lopez Ortiz, and A. Azevedo, Phys. Rev. B **89**, 014416 (2014).

[45] M. Schmid, S. Srichandan, D. Meier, T. Kuschel, J. M. Schmalhorst, M. Vogel, G. Reiss, C. Strunk, and C. H. Back, Phys. Rev. Lett. **111**, 187201 (2013).

[46] S. Y. Huang, W. G. Wang, S. F. Lee, J. Kwo, and C. L. Chien, Phys. Rev. Lett. **107**, 216604 (2011).

[47] D. Meier, D. Reinhardt, M. Schmid, C. H. Back, J.-M. Schmalhorst, T. Kuschel, and G. Reiss, Phys. Rev. B **88**, 184425 (2013).

[48] Y. Pu, E. Johnston-Halperin, D. D. Awschalom, and J. Shi, Phys. Rev. Lett. **97**, 036601 (2006).

[49] A. D. Avery, M. R. Pufall, and B. L. Zink, Phys. Rev. Lett. **109**, 196602 (2012).

[50] M. Hayashi, J. Kim, M. Yamanouchi, and H. Ohno, Phys. Rev. B **89**, 144425 (2014).

[51] C. O. Avci, K. Garello, M. Gabureac, A. Ghosh, A. Fuhrer, S. F. Alvarado, and P. Gambardella, Phys. Rev. B **90**, 224427 (2014).